

Resolution-induced anisotropy in LES

S. W. Haering[†], R. D. Moser^{†‡}

[†] Department of Mechanical Engineering, The University of Texas at Austin

[‡] The Institute for Computational Engineering and Science, The University of Texas at Austin

Large eddy simulation of complex geometries and domains often requires cells of high aspect ratio with varying shapes and orientations. The effects of such non-isotropic resolutions are often simplified or neglected in model formulation. Here, we examine resolution induced anisotropy and demonstrate that, for even isotropic turbulence, implicit grid filtering with anisotropic grids induces mild stress anisotropy along with potentially significant gradient-gradient anisotropy. A simple resolution scale-based model is constructed to potentially improve basic algebraic SGS behavior arising from anisotropic filters. This model, along with select existing SGS models, are evaluated using LES of forced HIT and compared to equivalently filtered inertial range theory.

1 Introduction

As computational resources improve and the demand for turbulence modeling accuracy in complex flows increases, large eddy simulation of engineering flows is expected to become common place. However, numerous challenges remain before LES can become a robust tool capable of supplanting RANS simulations in research and development applications. Since the advent of the dynamic approach [1], much LES research has focused on developing wall models to circumvent near-wall resolution requirements [2]. While this is certainly critical to enabling widespread usages of LES, other open issues remain.

In practical flows of engineering interest, the combination of high Reynolds number, complex geometry and limited computational resources often dictates discretization with relatively coarse highly anisotropic resolution that is changing rapidly in space. In such cases, the common assumptions of isotropic unresolved turbulence in equilibrium with the large scales and uniform filtering will often be violated. Though the issue of anisotropic resolution has been acknowledged in many SGS models [3–5], the specific issue has not been examined in detail. In this work, we examine the implications of anisotropic resolution and propose a simple treatment which has potential to be integrated into existing models. Before continuing, we briefly review existing resolution anisotropy treatments in the literature. Some of the models mentioned below are evaluated in §4.

In most cases, resolution anisotropy has been acknowledged through the definition of a scalar resolved length scale in terms of anisotropic resolution parameters. This resolved scale is then used in the formulation of subgrid models, such as the Smagorinsky model. A common example is the cube-root of a resolved cell volume, which in an orthogonal grid is given by $\Delta_{eq} = (\Delta_1 \Delta_2 \Delta_3)^{1/3}$, where Δ_i are resolution scales in each direction. However, scalar measures discard all the available information about cell anisotropy, shape, and orientation. Typically, such simplifications result in under-utilization of the available resolution in fine grid directions and/or excess of energy in the coarse grid directions, which is manifested as LES spectra that are not consistent with anisotropic filtering of real turbulence. In an attempt to alleviate the latter symptom, Scotti *et.al.* [3] introduced an additional scalar correction function to Δ_{eq} in the standard Smagorinsky model based on the ratio of the refined to most coarse grid dimensions to ensure the correct total dissipation. This is an improvement over the basic Smagorinsky model because it reduces artifacts of under-resolution in the coarse directions. However, this is at the cost of even worse under-utilization of available resolution in the fine directions. It appears that these simple model forms preclude LES that produce correct spectra with anisotropic resolution.

The Vreman model [4], which was primarily designed to ensure that the eddy viscosity vanishes in laminar regions, was the first to directly consider resolution anisotropy in its formulation. In this model, the eddy viscosity scales with the square root of the second invariant of a tensor composed of the velocity gradient contracted over a diagonal tensor with each component of the grid size squared. The magnitude of the resulting eddy viscosity depends on the velocity gradients as weighted by the grid anisotropy, which

reduces model viscosity where high gradients are accompanied by increased resolution and vice-versa. However, in the end, resolution anisotropy information is again discarded in favor of maintaining a scalar eddy viscosity. As shown in §4, the result is similar to basic Smagorinsky.

Rozema *et.al.* have more recently extended minimal dissipation models to account for grid anisotropy (AMD), without making a scalar filter width approximation like that described above [5]. Their model is motivated by the Poncaré inequality applied to anisotropic (rectilinear) grid cells, and is formulated to ensure that the eddy viscosity is sufficient to dissipate energy at the estimated rate of small-scale energy production. Here the anisotropy of the resolution enters into the estimate of the small-scale production. Despite some technical issues, the AMD model performs quite well with anisotropic resolution and is also examined in some detail in §4.

The vortex stretching subgrid stress model of Pullin *et.al.* [6] assumes the subgrid stress tensor is determined by a partial alignment of the total unresolved turbulent kinetic energy with the resolved strain rate orientation. Model anisotropy is prescribed by the resolved field while the total magnitude of τ_{ij} is determined directly from an integrated model of the unresolved energy spectrum. While not directly an eddy viscosity model, the alignment of the subgrid stress tensor using the resolved strain rate tensor results in nearly equivalent behavior. Further, as the scales of subgrid motion are embedded in the model for $E(k)$ and its integration from a single cutoff wavenumber, κ_c , to ∞ , filter anisotropy information is lost. A potential remedy would be to use a model for the full spectral energy density tensor with integration over individual cutoff wavenumbers.

Here, we develop a simple anisotropic tensor eddy viscosity subgrid model and evaluate its performance with anisotropic resolution relative to other SGS models, particularly AMD. The model is particularly simple in that the eddy viscosity does not fluctuate, though it does depend on statistical properties of the turbulence being simulated, in this case the dissipation. The characteristics of resolution-induced anisotropies in LES are discussed in §2, and our simple anisotropic subgrid model is introduced in §3. The performance of subgrid models for isotropic turbulence simulated with anisotropic resolution is explored in §4. Finally, concluding remarks are provided in §5.

2 Resolution-induced anisotropies

In a large eddy simulation with anisotropic resolution, the anisotropy of the resolution would be expected to produce anisotropy of the resolved and the subgrid Reynolds stresses. Of course, in homogeneous isotropic turbulence (HIT), the Reynolds stress is isotropic, and therefore dynamically insignificant. However, in an LES of HIT with anisotropic resolution, the resolved and subgrid Reynolds stress can be anisotropic, though their sum is still isotropic. To examine how the resolved and subgrid Reynolds stress anisotropy depend on resolution anisotropy, consider an idealized infinite Reynolds number isotropic turbulence with a $\kappa^{-5/3}$ inertial range spectrum starting at minimum wavenumber κ_m .

The expected stress anisotropy induced by anisotropic resolution in HIT may be studied by numerical integration of the spectral energy density tensor assuming a $\kappa^{-5/3}$ inertial range energy spectrum with integration limits corresponding to anisotropic cutoff wavenumbers

$$\langle \bar{u}_i \bar{u}_j \rangle = 2 \frac{C_k \varepsilon^{2/3}}{\pi} \int_{\kappa_m}^{\kappa_{c1}} \int_{\kappa_m}^{\kappa_{c2}} \int_{\kappa_m}^{\kappa_{c3}} |\kappa|^{-11/3} \left(\delta_{ij} - \frac{\kappa_i \kappa_j}{|\kappa|^2} \right) d\vec{\kappa} \quad (1)$$

and

$$\langle u'_i u'_j \rangle = 2 \frac{C_k \varepsilon^{2/3}}{\pi} \int_{\kappa_{c1}}^{\infty} \int_{\kappa_{c2}}^{\infty} \int_{\kappa_{c3}}^{\infty} |\kappa|^{-11/3} \left(\delta_{ij} - \frac{\kappa_i \kappa_j}{|\kappa|^2} \right) d\vec{\kappa} \quad (2)$$

where $\kappa_{c(i)} = \frac{L}{2\Delta_{(i)}}$ and L is set to 2π so the minimum wavenumber, κ_m , is unity. Throughout this work, only cell shapes of two repeating coarse directions and two repeating fine directions are considered. These limiting cases are labeled “book” and “pencil” cells, respectively. All other cell shapes would exhibit behavior in between these cases. Book type cells are particularly interesting as they are common in near-wall regions of a simulation grid. Pencil type cells are typically used more sparingly but do often appear in critical regions such as near stagnation and separation points of 2D bodies.

For isotropic turbulence with anisotropic grid filtering, the subfilter turbulent stress is weakly anisotropic in expectation (Fig. 1a) with anisotropy saturating at grid aspect ratios of about (32 : 1). However, the

saturating anisotropy increases with the ratio coarsest filter size to minimum wavenumber; such conditions are seen in a relatively coarse LES. Pencil cells show significantly more anisotropy than book cells. Perhaps more importantly to LES, the resolved stress anisotropy (Fig. 1b) similarly saturates at the same grid aspect ratio and is only significant when the coarsest filter size is nearly the minimum wavenumber. When this ratio is at least 16, the resolved anisotropy is negligible.

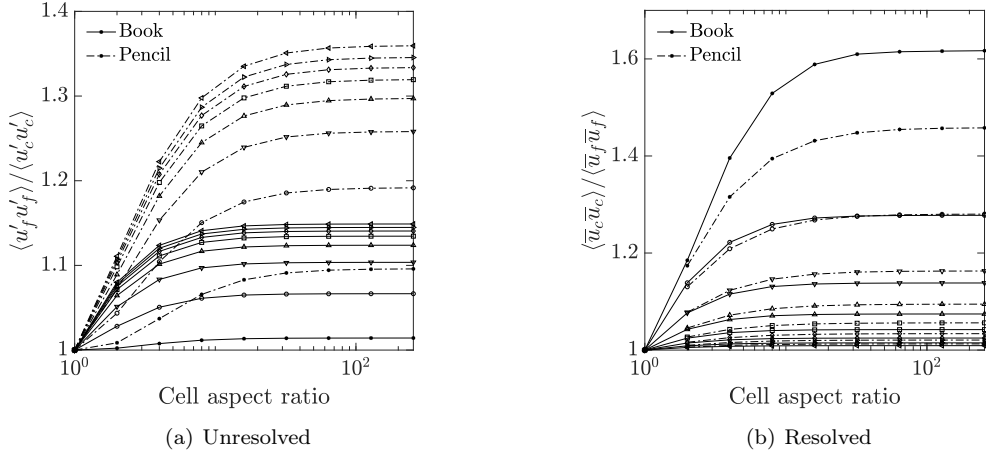


Figure 1: Expected resolution-induced stress anisotropy of unresolved (a) and resolved (b) scales for a $k^{-5/3}$ inertial range energy spectrum. Values are computed by integration of the spectral energy density tensor from $k_m = 1$ to k_c and k_c to a converged value, where k_c corresponds to the anisotropic resolution specified filter size. Symbols indicate the ratio of the coarsest wavenumber to k_m as follows: $2^*, 4^o, 8^{\nabla}, 16^{\Delta}, 32^{\square}, 64^{\diamond}, 128^{\triangleright}, 256^{\triangleleft}$. Subscript “c” indicates the coarse direction while “f” indicates the fine direction.

Given the resolution-induced stress anisotropy of the expected stresses is only mildly anisotropic, it is tempting to neglect resolution anisotropy entirely. However, all SGS models proposed to date are formed with information from the resolved gradient tensor, examining the expected gradient anisotropy is therefore necessary. Where the local grid size is not much smaller than the integral length scales, the SGS model will be required to represent these mildly anisotropic stresses using gradient anisotropy [7]. Further, SGS models are required to model the correct transfer of energy from resolved to unresolved scales of motion. This necessarily involves at least the velocity gradient-gradient product for any eddy-viscosity SGS model and so the induced velocity component anisotropy is not explicitly relevant for this function.

The expected gradient-gradient anisotropy induced by anisotropic resolution in HIT is calculated by taking the gradient twice of the spectral energy density tensor and again integrating over anisotropic filter widths and noting $\langle \bar{u}_i \partial_k \partial_l \bar{u}_j \rangle = \langle \partial_k \partial_l \bar{u}_i \bar{u}_j \rangle = 0$,

$$\mathcal{G}_{ijkl} = \langle \partial_k \bar{u}_i \partial_l \bar{u}_j \rangle = 2 \frac{C_k \varepsilon^{2/3}}{\pi} \int_{\kappa_m}^{\kappa_{c1}} \int_{\kappa_m}^{\kappa_{c2}} \int_{\kappa_m}^{\kappa_{c3}} \kappa_k \kappa_l |\kappa|^{-11/3} \left(\delta_{ij} - \frac{\kappa_i \kappa_j}{|\kappa|^2} \right) d\vec{\kappa}. \quad (3)$$

With \mathcal{G}_{ijkl} being non-zero only when $i = j$ and $k = l$, and again only examining the limits of book and pencil cells, only three unique eigenvalues of \mathcal{G}_{ijkl} result as shown in Fig. 2

The expected gradient for HIT is, of course, zero as is its anisotropy. However, \mathcal{G}_{ijkl} provides the variance of the gradient tensor and if the eddy viscosity is uncorrelated with the velocity gradient, it directly provides the model dissipation anisotropy. The most salient result from the theoretical inertial range \mathcal{G}_{ijkl} is that, while the gradient-gradient anisotropy saturates similarly to stress for book cells, it exponentially increases with cell aspect ratio for pencil cells. Constructing a stress anisotropy which saturates (Fig. 1) at relatively low aspect ratios using timescales provided directly from \mathcal{G}_{ijkl} becomes problematic and suggests both the cell anisotropy and shape must be directly incorporated into the model.

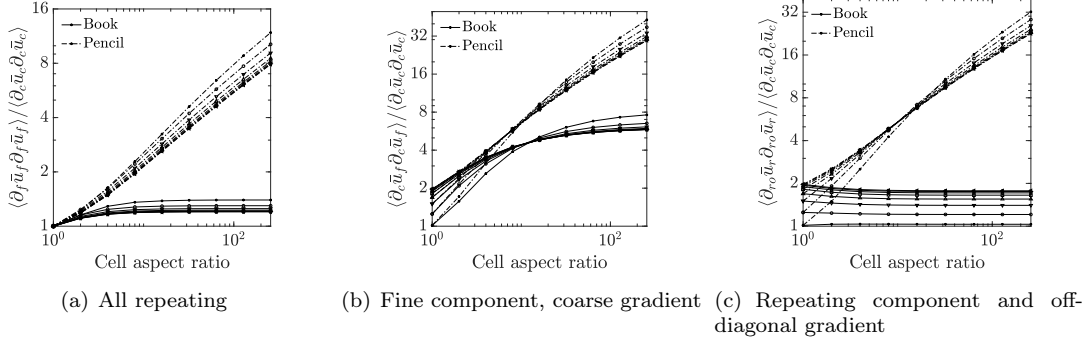


Figure 2: Expected resolution-induced gradient-gradient anisotropy of the resolved scales for a $k^{-5/3}$ inertial range energy spectrum. Values are computed by integration of the second gradient of the spectral energy density tensor from $k_m = 1$ to k_c where k_c corresponds to the anisotropic resolution specified filter size. Symbols indicate the ratio of the small resolved wavenumber to the coarsest cutoff wavenumber to as follows: $2^*, 4\circ, 8\nabla, 16\Delta, 32\square, 64\Diamond, 128\triangleright, 256\triangleleft$. Subscript “c” indicates the coarse direction while “f” indicates the fine direction and “ro” indicates repeating off-diagonal component.

The effects of neglecting resolution anisotropy and the resulting gradient anisotropy can be demonstrated with the basic Smagorinsky model [8] applied to simulations with anisotropic resolutions. In these simulations, and elsewhere in this paper, LES of forced periodic HIT at infinite Re is performed with modified version of the dealiased psuedo-spectral code Poongback [9]. All spectra are averaged with 10 samples over at least four eddy turnover times. Comparisons are made with equivalently filtered $\kappa^{-5/3}$ theoretical inertial range energy spectra (Fig. 3 & 4). Cell aspect ratios of (4 : 1) up to (32 : 1) are considered. For both limits of cell aspect ratio, an excess of energy is present in low and mid wavenumbers with a depletion of energy at the finest scales. In particular, the coarse direction sees approximately six times surplus of turbulent kinetic energy at the cutoff for the highest aspect ratio considered. The energy pile-up at the coarse direction cutoff appears to nearly saturate at the highest cell aspect ratio considered here (32 : 1) for both book and pencil cells.

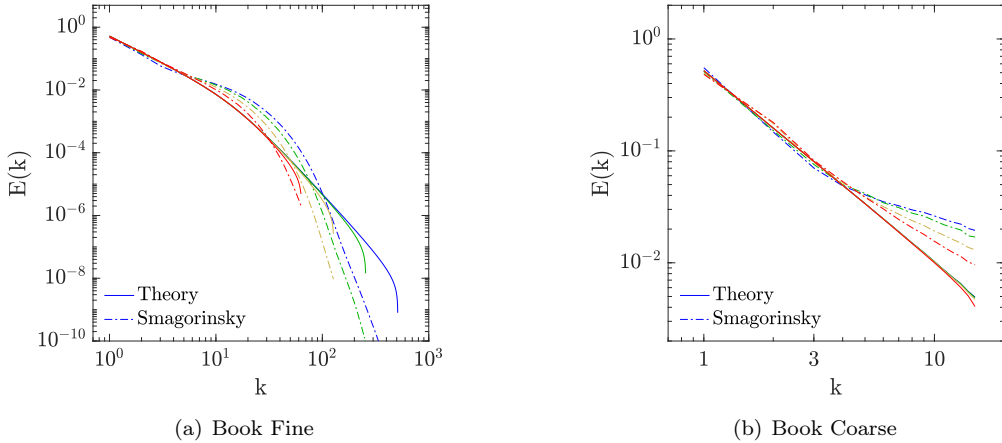


Figure 3: Directional energy spectra, normalized by $\varepsilon^{2/3} \kappa_{min}^{-5/3}$, of the standard Smagorinsky model with anisotropic book resolution and equivalently filtered theoretical $k^{-5/3}$ energy spectra.

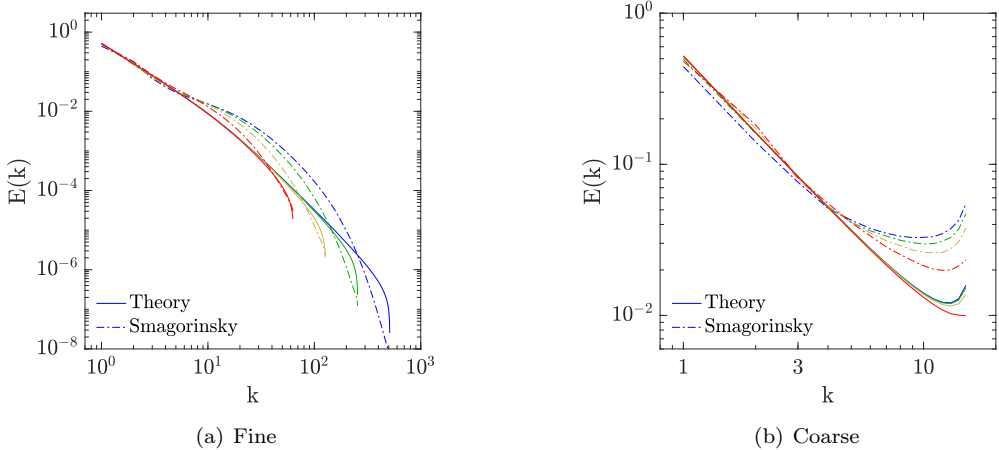


Figure 4: Directional energy spectra of pencil cells, normalized by $\varepsilon^{2/3} \kappa_{min}^{-5/3}$, of the standard Smagorinsky model with anisotropic resolution and equivalently filtered theoretical $k^{-5/3}$ energy spectra.

Note that using the dynamic approach [1] would not improve these results as the effects of resolution anisotropy would be lost to averaging over all homogeneous directions. It may be possible to construct a tensor-based dynamic coefficient to correct this issue but such an approach has not been explored here. The anisotropy correction of Scotti *et.al.* [3] is considered later.

As previously discussed, these tests do not directly evaluate effects of mean turbulent stress. It seems likely that the energy spectra distortion is purely a result of incorrectly modeling the dissipation anisotropy. This hypothesis is examined later. With the energy input fixed through low wavenumber stirring, the field and its gradients are forced to adjust to produce the correct total dissipation. The resulting resolved turbulent structures, and their associated momentum transfer, are also distorted. In a non-trivial LES with non-vanishing transport terms, errors in the convective derivative result. Roughly, transport of resolved momentum by large structures is enhanced while simultaneously reducing the transport by the fine structures. Constructing models to precisely reproduce the expected dissipation anisotropy is therefore of paramount importance. Here, we attempt to construct a model which perform adequately in the presence of grid anisotropies using other considerations.

3 A simple anisotropic subgrid model

We begin by relaxing isotropy assumptions on standard eddy viscosity models so the modeled diffusivity approximating the effects of the unresolved turbulence may take on directional dependance. With an anisotropic eddy viscosity, the standard SGS model must be modified accordingly. The simplest model for the deviatoric portion of the subgrid stress tensor τ_{ij} in terms of ν_{ij} is given by

$$\tau_{ij} - \frac{2}{3} \tau_{kk} \delta_{ij} \approx \nu_{jk} \partial_k \bar{u}_i + \nu_{ik} \partial_k \bar{u}_j \quad (4)$$

where the directional dependence in the modeled turbulent diffusivity specifically acts on each directional change in the filtered velocity field. Under the conditions of an isotropic and diagonal eddy viscosity, (4) collapses to the standard Boussinesq eddy viscosity model. However, where this is not true, the principle axis of the SGS tensor are no longer assumed to be aligned with those of the filtered strain tensor and may be affected by the anisotropy in the filter itself and the entire velocity gradient tensor. While the model for τ_{ij} is still symmetric, the magnitude may now include contributions from rotational deformation rates.

Second, we adopt a more rich description of the underlying grid in the form of the resolution tensor, \mathcal{M}_{ij} , which is formally the symmetric portion of the Jacobian defining the mapping of a unit cube to a

physical cell or the square-root of the cell metric tensor [10]. The eigenvalues of \mathcal{M}_{ij} therefore represent the size of the cell while its eigenvectors provide its orientation. For all orientations and locations in a domain, \mathcal{M}_{ij} provides the implicit filter-scale separation vector as $r_i(\mathbf{e}, \mathbf{x}) = \mathcal{M}_{ij}(\mathbf{x})e_j$. It follows that contraction with the gradient index of the resolved gradient tensor, $(\mathcal{M}_{ik}\partial_k \bar{u}_j)$, has the natural interpretation as the filtered velocity field difference tensor at separations defined by the resolution. Taking the inner product with itself, $(\mathcal{M}_{im}\partial_m \bar{u}_k \mathcal{M}_{jn}\partial_n \bar{u}_k)$, an anisotropic measure of the filtered second-order structure function is formed. Common grid measures are invariants or eigenvalues of \mathcal{M}_{ij} , *e.g.* $\delta_{min} = \min(\lambda_i^{\mathcal{M}})$, $\delta_{diag} = (\mathcal{M}_{ij}\mathcal{M}_{ji})^{1/2}$, $\delta_{vol} = (\det(\mathcal{M}))^{1/3}$, *etc.* The resolution tensor is a more complete representation of the grid than scalar measures allowing for models composed of it to not discard any resolution information related to size, shape, and orientation. SGS models become operationally consistent making such models valid not only where the grid orientation is aligned global coordinate system and obviates ambiguous scalar cell measures.

Eddy viscosity anisotropy used in (4) should satisfy

$$\langle \varepsilon_{ij} \rangle = \langle \nu_{ik}\partial_j \bar{u}_l \partial_k \bar{u}_l \rangle + \langle \nu_{jk}\partial_i \bar{u}_l \partial_k \bar{u}_l \rangle + \langle \nu_{lk}\partial_j \bar{u}_l \partial_k \bar{u}_i + \partial_i \bar{u}_l \partial_k \bar{u}_j \rangle, \quad (5)$$

where $\langle \varepsilon_{ij} \rangle$ is the expected directional contribution to the total dissipation, $(\langle \partial_j \bar{u}_k \tau_{ik} \rangle + \langle \partial_i \bar{u}_k \tau_{jk} \rangle)$. Taking the trace of (5) and using homogeneous directional averaging as the expectation operation would lead to something like the dynamic approach with the effects of resolution anisotropy being lost. Instead, we proceed with an expected eddy viscosity allowing ν_{ij} to be pulled out of the operator. Further, for isotropic turbulence, the expected model anisotropy can only depend on the eigenvalues of \mathcal{M}_{ij} so that the system of equation in (5) becomes uncoupled when aligned with the cell coordinate system allowing solution of each eigenvalue of ν_{ij} independently. Thus, with $\mathcal{G}_{ijkl} = \langle \partial_k \bar{u}_i \partial_l \bar{u}_j \rangle$ and again noting \mathcal{G}_{ijkl} is only non-zero when $i = j$ and $k = l$, (5) may be rearranged as

$$\lambda_{(i)}^{\nu} = \lambda_{(i)}^{\varepsilon} \left(\lambda_{jj(i)(i)}^{\mathcal{G}} + \lambda_{(i)(i)(i)(i)}^{\mathcal{G}} \right)^{-1}, \quad (6)$$

where subscripts in a (\cdot) indicate no summation of repeating indices. While \mathcal{G}_{ijkl} may be found by numerical integration for an inertial range energy spectrum as shown in the previous section, anisotropy of ε_{ij} requires a model for the single-point triple correlation and will be the subject of future work.

As a first-order approximation, the isotropic limiting behavior of the eddy viscosity anisotropy is readily found for isotropic resolution in an inertial range. In this most basic case, the spectral representation of \mathcal{G} for a $k^{-5/3}$ energy spectrum (3) reduces to

$$\mathcal{G}_{kk(i)(i)} = \frac{1}{2} C_k \varepsilon^{2/3} (\kappa_c^{4/3} - \kappa_m^{4/3}) \quad (7)$$

and

$$\mathcal{G}_{(i)(i)(i)(i)} = \frac{1}{10} C_k \varepsilon^{2/3} (\kappa_c^{4/3} - \kappa_m^{4/3}) \quad (8)$$

where $\kappa_c = \pi/\Delta$, $\kappa_m = 2\pi/L$, and L is the domain size. Further simplifying the solution of (6) is the fact that $\langle \varepsilon_{ij} \rangle$ is, of course, isotropic in this limit. Naturally, this length scaling is a crude approximation and cannot be expected to accurately produce the correct eddy viscosity anisotropy for all resolution anisotropies. However, the correct total dissipation can be built into the model through a scalar coefficient which can only be a function of the eigenvalues of \mathcal{M}_{ij} and L . The basic model takes the form

$$\lambda_i^{\nu} = C(\mathcal{M}) \varepsilon^{1/3} ((\lambda_i^{\mathcal{M}})^{-4/3} - (L_i/2)^{-4/3})^{-1}, \quad (9)$$

To reduce the complexity of $C(\mathcal{M})$, the effects of the minimum resolved wavenumber may be neglected yielding the basic “M43” model

$$\nu_{ij} = C(\mathcal{M}) \varepsilon^{1/3} \mathcal{M}_{ij}^{4/3}, \quad (10)$$

where $C(\mathcal{M})$ is only a function of two of the eigenvalues of \mathcal{M}_{ij} scaled by the third. The simplification in (10), is valid for cases of the coarsest cutoff wavenumber being much larger than the smallest resolved wavenumber. Alternatively, the parameter dependance of $C(\mathcal{M})$ may be approximately reduced without complete neglect of L by shifting the eigenvalues of \mathcal{M}_{ij} to create a modified metric tensor, \mathcal{M}^* , with eigenvalues of $((\lambda_i^{\mathcal{M}} - (L_i/2))^{-1}$. Replacing \mathcal{M} with \mathcal{M}^* in (10) also requires a different $C(\mathcal{M})$ and is referred to as the “M43 low-k” model. The fitting procedure for $C(\mathcal{M})$ is provided in the appendix. Currently, these fits are algebraically tedious and will be streamlined in future work.

4 Evaluation

In addition to the proposed M43 model and its variant, we examine the AMD model in detail due to its exceptional performance in the presence of anisotropic resolution. Whereas the M43 model effectively specifies a *single* eddy viscosity *ab-initio* which is used at every cell for the entirety of the HIT simulation, the AMD model makes use of a highly non-linear eddy viscosity in the instantaneous and local velocity gradient tensor along with clipping to establish the correct local dissipation. These two models therefore represent the opposite ends of the spectrum and achieve nearly identical results in terms of resolved energy spectra.

Other models considered due to their accounting for cell anisotropy and shape include the modified Smagorinsky model of Scotti and the Vreman model. However, as these exhibit similar deficiencies as the basic Smagorinsky model (Fig. 3), we only provide single high-aspect ratio examples.

4.1 Directional Energy Spectra

As with the example basic Smagorinsky model in §, models are evaluated by their ability to reproduce the correct energy distribution of filtered isotropic inertial range turbulence by performing LES of infinite Re forced periodic HIT with anisotropic resolution (Fig. 5-13). Using filtered theoretical $k^{-5/3}$ energy spectrum allows evaluation of the effects of resolution anisotropy free of finite Re effects. This is critical for examining high aspect ratio cells where both the lowest and highest cutoff wavenumbers, as dictated by the cell, must be in the inertial range. All filters performed here correspond to sharp spectral ellipsoidal filters with Nyquist frequencies discarded as opposed to more standard box filtering. By using the former filter type, wavenumbers whose magnitudes are strongly dissipated by realspace eddy viscosity models are excluded. Directional energy spectra, as opposed to radial, are examined to more directly reveal the anisotropic effects of the resolutions considered. LES are performed with the 3/2-dealiased pseudospectral code PoongBack. Negative viscosity forcing is performed over a band of wavenumber magnitudes $|\kappa| = (0.0, 2.0]$. All statistics are taken from 10 samples over at least four eddy turnover times after being brought to a steady-state. Additional CFL constraints are discussed in the appendix. All models considered yield virtually identical results for isotropic grids as such, these results are not shown.

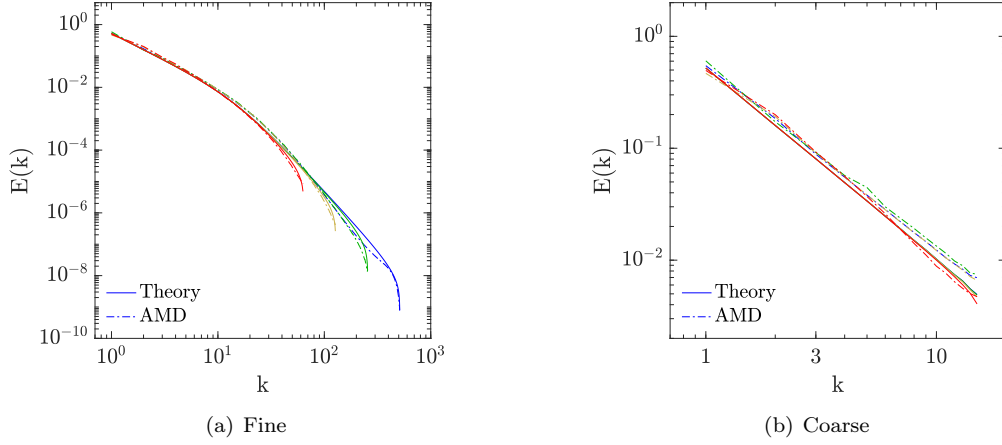


Figure 5: AMD model directional energy spectra with book cells, normalized by $\varepsilon^{2/3} \kappa_{min}^{-5/3}$ and equivalently filtered theoretical $k^{-5/3}$ energy spectra.

We begin by performing the same book and pencil cell evaluations up to aspect ratios of (32 : 1) as for the basic Smagorinsky model (Fig. 3 and 4). The AMD model results are shown in Fig. 5 and 6 with M43 and M43 low-k shown in Figures 7, 8 and 9, 10. All three of these models perform quite well in comparison

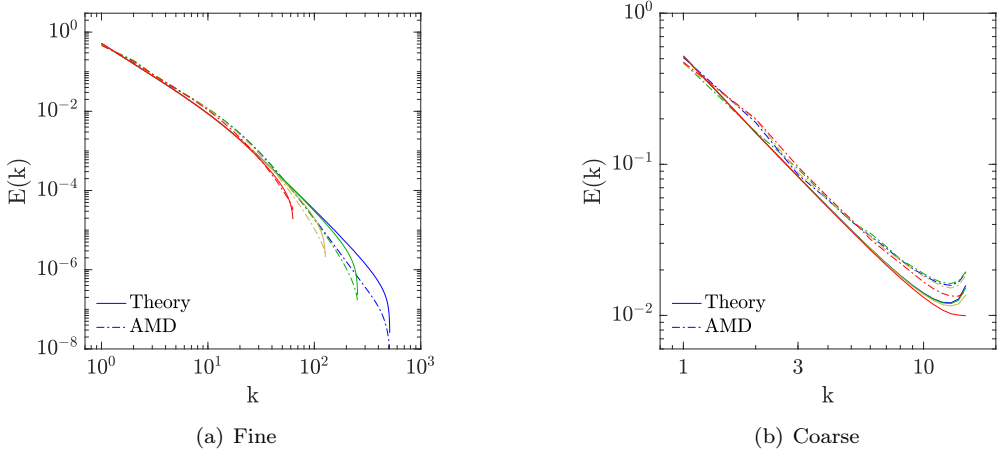


Figure 6: AMD model directional energy spectra with pencil cells, normalized by $\varepsilon^{2/3} \kappa_{min}^{-5/3}$ and equivalently filtered theoretical $k^{-5/3}$ energy spectra.

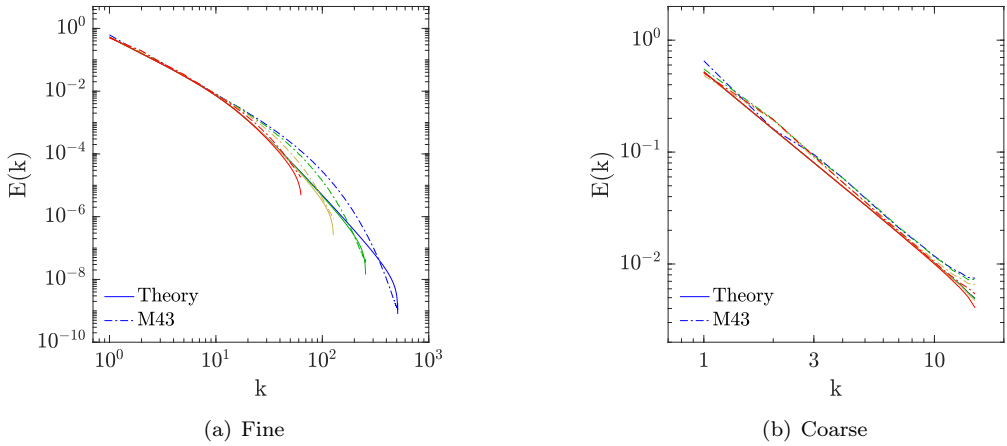


Figure 7: M43 model directional energy spectra with book cells, normalized by $\varepsilon^{2/3} \kappa_{min}^{-5/3}$ and equivalently filtered theoretical $k^{-5/3}$ energy spectra.

to Smagorinsky with little to no energy pile-ups at the cutoff in the coarse direction. A small and seemingly rapidly (in terms of increasing aspect ratio) saturating energy excess is exhibited by the AMD model in the coarse direction particularly for pencil cells. Moderate amounts of mid-range wavenumber energy excess is seen for the M43 model which is reduced in the low- k version for both cell types but does appear to increase with cell aspect ratio. All models are slightly overly dissipative at the highest wavenumbers in the fine directions with the M43 low- k model being the most significant.

Next, we examine model performance as a function of the coarsest cutoff wavenumber, κ_{cc} , to minimum resolved wavenumber, κ_m , with a fixed cell aspect ratio of (8 : 1) for book cells only (Fig. 11). Ratios of κ_{cc}/κ_m considered are (2 : 1), (4 : 1), (8 : 1), and (16 : 1). The basic Smagorinsky model is also evaluated for reference (Fig. 11a). We see that the previously observed coarse cutoff energy pileup observed for Smagorinsky increases relative to the total resolved energy as κ_{cc}/κ_m is reduced. Once again, the proposed models and AMD vastly out-perform Smagorinsky and yield nearly theoretical results. The low- k version of the M43 model is successful in reducing the mid-range wavenumber excess energy in the fine directions

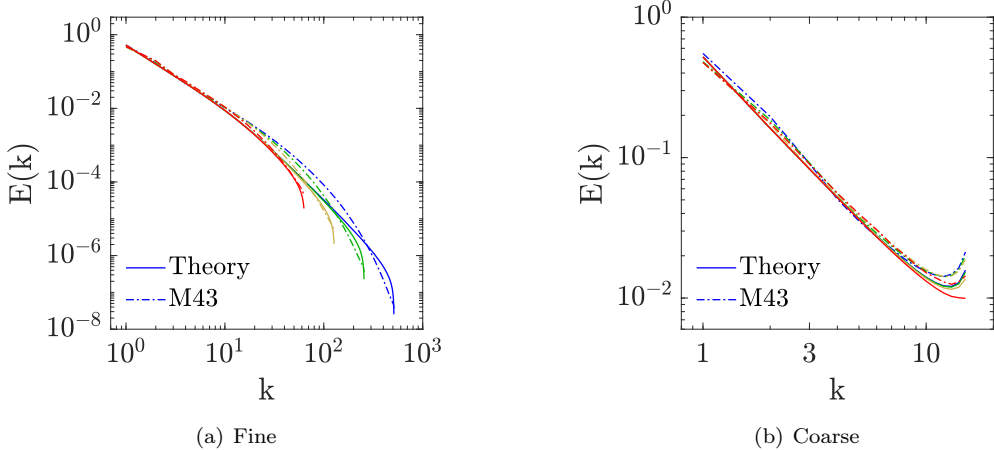


Figure 8: M43 model directional energy spectra with pencil cells, normalized by $\varepsilon^{2/3} \kappa_{min}^{-5/3}$ and equivalently filtered theoretical $k^{-5/3}$ energy spectra.

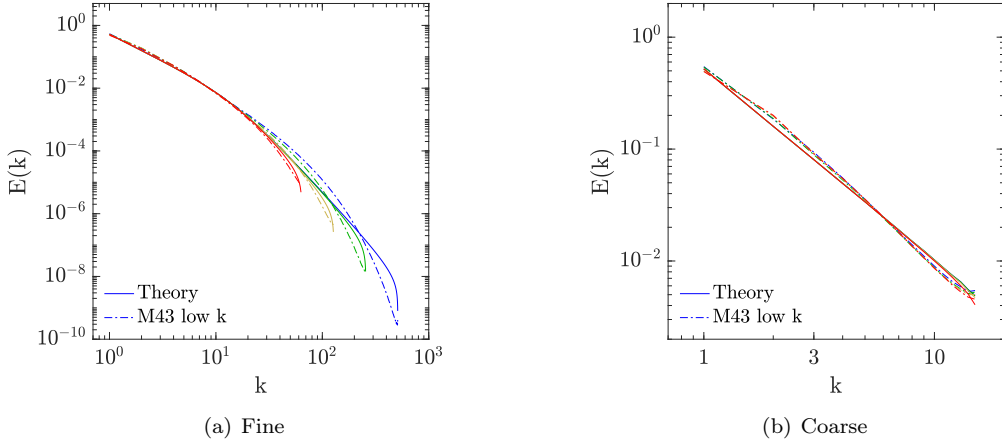


Figure 9: M43 low k model directional energy spectra with book cells, normalized by $\varepsilon^{2/3} \kappa_{min}^{-5/3}$ and equivalently filtered theoretical $k^{-5/3}$ energy spectra.

in comparison to the basic M43 model. However, by the highest κ_{cc}/κ_m considered, both M43 variants are nearly identical.

Finally, we briefly discuss the Vreman (Fig. 12) and Scotti Smagorinsky (Fig. 13) variant. For both models, the qualitative performance is similar to the basic Smagorinsky with coarse direction and mid-range fine direction energy pile-up and under-utilization of the available high-range fine direction wavenumbers. As the Vreman model was primarily designed to cause the model viscosity to vanish in laminar regions, poor results in the presence of anisotropic grids is not surprising. The modified Smagorinsky effectively increases the model constant in response to the cell aspect ratio and shape. Naturally, it cannot improve the basic anisotropic resolution behavior of the Smagorinsky model and can only reduce energy pile-ups by shifting the magnitude of the total dissipation away from the total gradients and to the model coefficient. This is precisely the observed behavior. However, especially for pencil cells, it appears the correction should be enhanced.

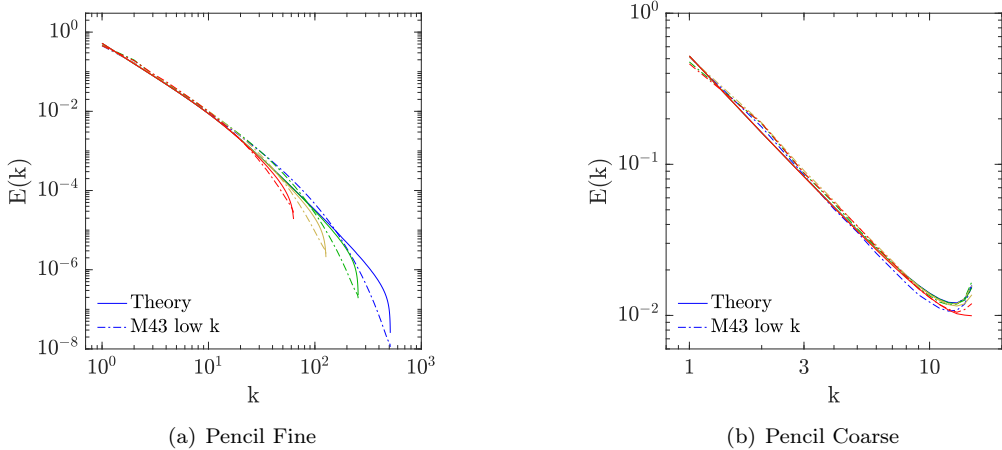


Figure 10: M43 low k model directional energy spectra with pencil cells, normalized by $\varepsilon^{2/3} \kappa_{min}^{-5/3}$ and equivalently filtered theoretical $k^{-5/3}$ energy spectra.

4.2 Dissipation anisotropy

A comparison between the characteristics of the M43 and AMD models may be instructive to the general formulation of SGS models as they are so different in construction yet yield similar results in the presence of anisotropic resolution. That is, they must share some common feature that other models do not. As the divergence of the actual model terms are necessarily zero in HIT, the stress is not the relevant diagnostic. The most obvious candidate for this shared features is the directional contribution to the energy dissipation, or $\langle \varepsilon_{ij} \rangle = \langle \partial_i \bar{u}_k \tau_{kj} \rangle$. Normalized eigenvalues of $\langle \varepsilon \rangle_{ij}$ are shown in Fig. 14 for M43 low- k , AMD, and Smagorinsky.

For both cell shape limits, the majority of M43 dissipation is due to gradients in the coarse resolution direction. For book cells, this trend is so pronounced that gradients in the fine direction become slightly anti-dissipative at (16 : 1) cell aspect ratios. Smagorinsky produces the opposite behavior with the majority of the dissipation coming from gradients in the fine direction. AMD, however, yields nearly equivalent contributions to the total dissipation from all gradient directions for all aspect ratios. Thus, the nearly equivalent spectral energy distribution resulting from M43 and AMD is not due directional dissipation contributions.

5 Conclusions

Specific and general treatments of resolution anisotropy in LES have been largely neglected. While not the primary impedance to the widespread use of LES, models which respect complex grid topology are a necessity before replacing RANS as the standard engineering tool for simulation of turbulent flows. Here, we have examined some of the implications of implicit grid filtering with anisotropic resolution on both stress and resolved gradient-gradient anisotropies. While induced anisotropy in the stress may be small and saturating with cell aspect ratio, resolved gradient-gradient anisotropies exponentially grow with cell aspect ratio for all but the limiting case of book-type cells. Thus, expecting a scalar eddy viscosity based SGS model to represent stress anisotropies using gradient information seems unlikely unless the eddy viscosity is uncorrelated with the velocity gradient tensor, by construction. We have demonstrated typical shortcomings of existing SGS models used with anisotropic resolution: large pileups of energy in the vicinity of the coarse direction cutoff along with under utilization of the fine resolution directions with associated waste of computational expense. Using theoretical behavior in the limit of isotropic cells, we have constructed a simple tensor-based eddy viscosity model which performs remarkably well when used with anisotropic resolutions. In the process, we have advocated for discarding arbitrary scalar grid measures in favor the

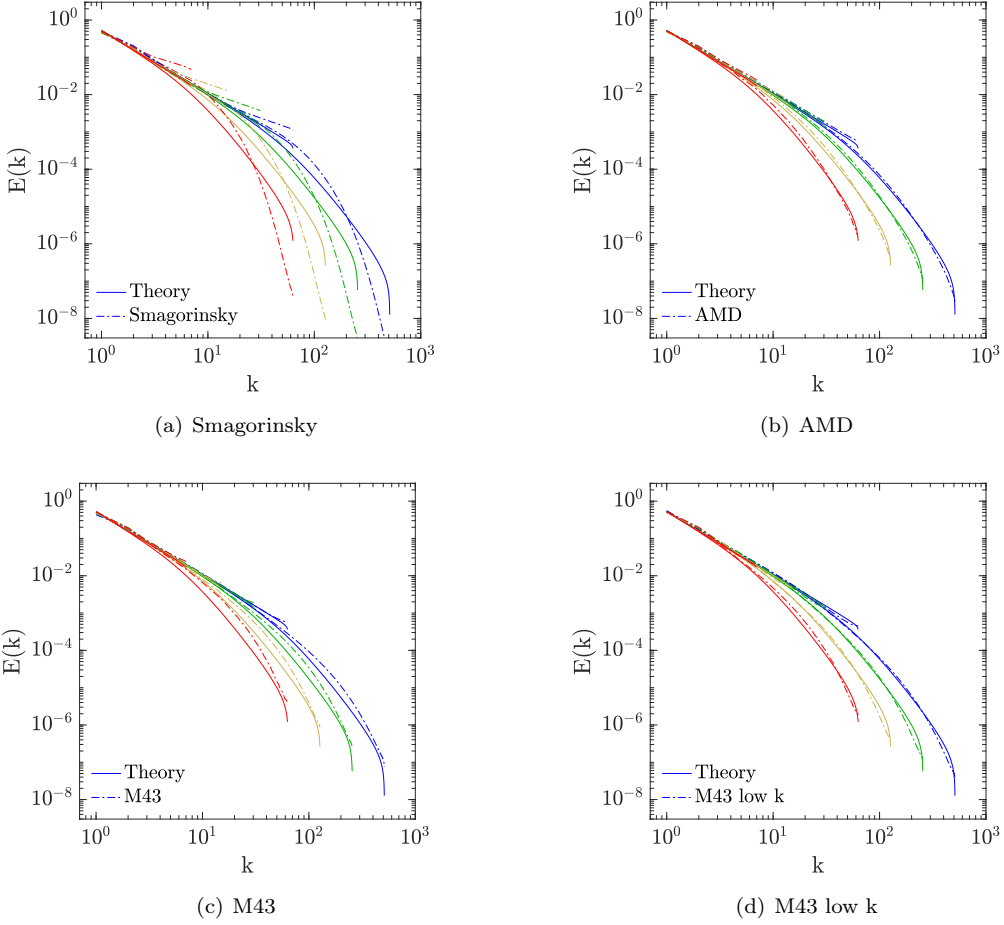


Figure 11: Directional energy spectra with book cells at ratios of minimum cutoff to minimum resolved wavenumbers of (2 : 1) to (16 : 1) with a fixed aspect ratio of (8 : 1), normalized by $\varepsilon^{2/3} \kappa_{min}^{-5/3}$ and equivalently filtered theoretical $k^{-5/3}$ energy spectra.

resolution tensor when formulating SGS models for both the inherent complete resolution description and the resulting operational consistency which makes such models valid for any local cell orientation. The proposed eddy viscosity model requires only the local resolution and the expected dissipation. It is therefore simple to construct but requires information, in the dissipation, which may not be readily available in non-trivial simulations. Spectral energy distributions in tests of HIT resulting from this single, ab-initio, tensor eddy viscosity are comparable to those of the AMD model while greatly out-performing other existing SGS models. However, what makes these two significantly different models perform similarly remains illusive as their contributions to the total dissipation was found to be drastically different. While the proposed model may not see wide-spread application due to its reliance on knowledge of the local mean dissipation and algebraically tedious constant, it represents a useful step in the the development of complex SGS models as it both introduces relatively simple construction of anisotropic turbulent diffusivities and illustrates how representing the subgrid stress anisotropy is effectively divorced from representing the resolved dissipation anisotropy with eddy viscosity models in an LES.

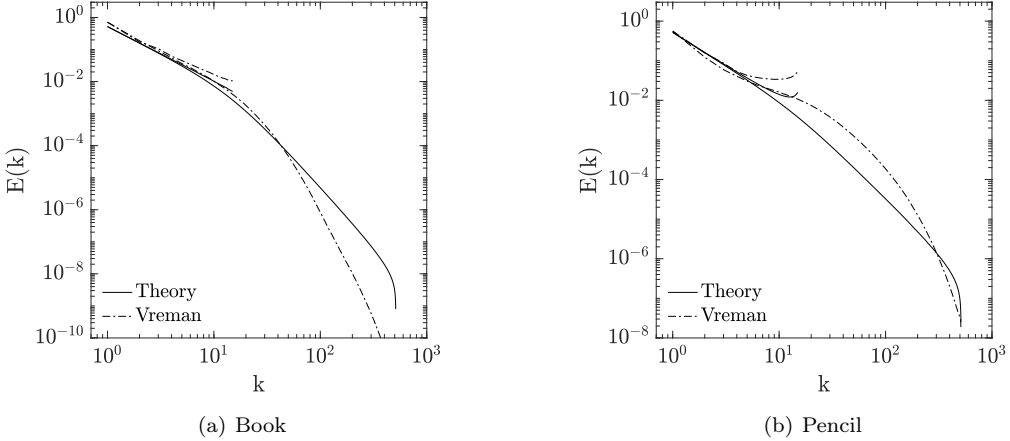


Figure 12: Vreman model directional energy spectra at cell aspect ratio of (32 : 1), normalized by $\varepsilon^{2/3} \kappa_{min}^{-5/3}$ and equivalently filtered theoretical $k^{-5/3}$ energy spectra.

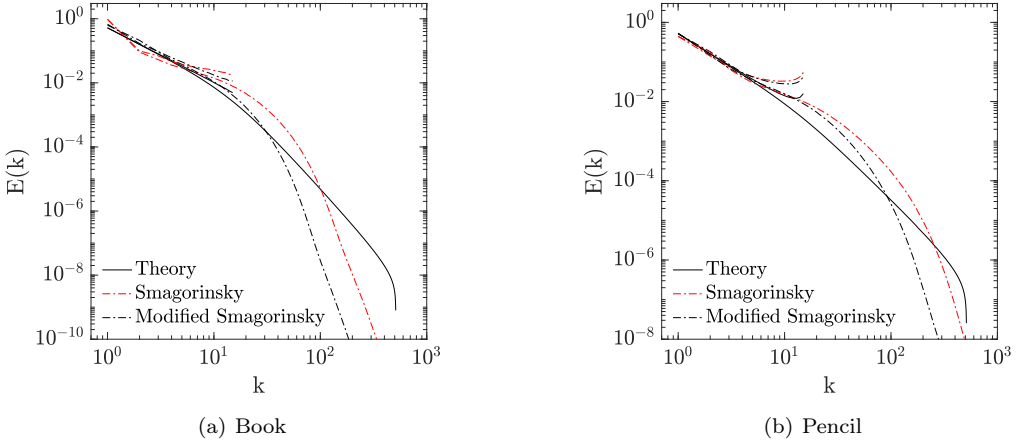


Figure 13: Modified and basic Smagorinsky models directional energy spectra at cell aspect ratio of (32 : 1), normalized by $\varepsilon^{2/3} \kappa_{min}^{-5/3}$ and equivalently filtered theoretical $k^{-5/3}$ energy spectra.

Appendix A: M43 coefficient

Let \mathbb{G} be the normalized expected filtered velocity gradient-gradient product

$$\mathbb{G}_{ijkl} = \mathcal{G}_{ijkl} \varepsilon^{-2/3} \delta^{4/3} \quad (11)$$

where δ is the minimum eigenvalue of the resolution scale tensor, \mathcal{M}_{ij} . For isotropic turbulence, we may evaluate (11) numerically for a wide range of anisotropic resolutions by assuming a Kolmogorov inertial range using (3). Note that the effective wavevectors corresponding to the gradient operator for the particular numerical method should be used. With the spectral code used here, these operators are exact. The upper limit of the integral is also dependent on the numerics; for PoongBack, k_c corresponds to a sharp spectral box filter with the Nyquist frequencies discarded. The lower limit is here defined by the smallest resolved wavenumber as dictated by the box size but would loosely correspond to the integral length scale for more complex flows. For each cell shape (different \mathcal{M}), integration of (3) yields 9 positive

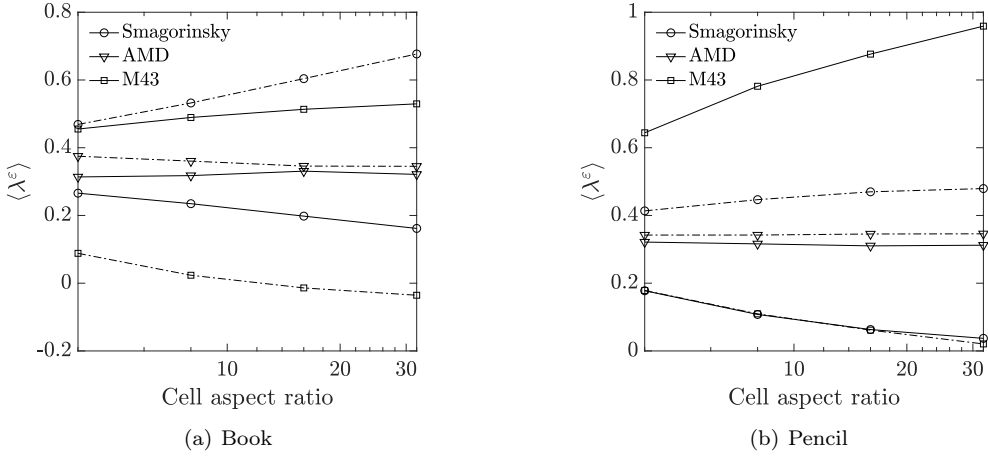


Figure 14: Mean directional contribution to the total dissipation with using the basic Smagorinsky, AMD, and M43 low-k models from cell aspect ratio of (4 : 1) to (32 : 1), normalized by $\langle \varepsilon \rangle$. Coarse resolution gradient directions are shown with (—) while fine are shown with (—·).

eigenvalues with all other index combinations of \mathbb{G}_{ijkl} being zero in expectation.

Contractions of the grad-grad product with (5) and (10) with the assumption of isotropic ε_{ij} yield model coefficients which satisfy the requirement that the constructed eddy viscosity and SGS model produce the correct total expected dissipation for any combination cell aspect ratio and shape. In this fully contracted form, Cayley-Hamilton theory and eigenvector alignment tell us the eigenvalues of ν_t are representable entirely as functions of $\lambda_{\mathcal{M}}$ and L and hence, so are the model coefficients. The number of dependancies are reduced by two as described in the §3.

Fourth-order polynomials of the scaled eigenvalues of \mathcal{M} expressed as $r = (a^2 + b^2)^{1/2}$ and $\theta = \cos^{-1}(max(a, b)/r)$ with $a = \lambda_{\neq norm+1}^{\mathcal{M}}$ and $b = \lambda_{\neq norm-1}^{\mathcal{M}}$, i.e. the other two eigenvalues not δ_{norm} (though these may be repeating) and $y = \ln(\sin(2\theta))$, $x = \ln(r)$ with

$$\begin{aligned}
 C(\mathcal{M}) = C_{\mathcal{M}}^o & (c_1 + \\
 & c_2 x + c_3 y + \\
 & c_4 x^2 + c_5 x y + c_6 y^2 + \\
 & c_7 x^3 + c_8 x^2 y + c_9 x y^2 + c_{10} y^3 + \\
 & c_{11} x^4 + c_{12} x^3 y + c_{13} x^2 y^2 + c_{14} x y^3 + c_{15} y^4)
 \end{aligned} \tag{12}$$

where $C_{\mathcal{M}}^o$ is an overall coefficient used to calibrate the model for isotropic resolution. For spectral numerics we find for M43 low-k model

$$\begin{aligned}
 c = (1.0, -0.06318, -0.06453, 0.1387, -0.006091, 0.08502, -0.03956, -0.01467, \\
 -0.006863, 0.03360, 0.003345, 0.001996, 0.001173, 0.001305, 0.004430)
 \end{aligned}$$

with $C_{\mathcal{M}}^o = 0.0348$ and for the basic M43 model

$$\begin{aligned}
 c = (1.0, -0.07345, -0.05307, 0.1446, -0.001129, 0.09822, -0.04086, -0.01575, \\
 -0.005824, 0.03826, 0.003444, 0.002086, 0.001145, 0.001463, 0.004995)
 \end{aligned}$$

with $C_{\mathcal{M}}^o = 0.0606$. Naturally, the use of polynomials to fit the coefficients limits their applicability to the range of fitting data. The above coefficients make us of data up to (128 : 1) aspect ratio cells.

Appendix B: Additional time step requirements

Using standard CFL timestep constraints [11], all models exhibit sharp pileups of energy at the fine cutoff with magnitude increasing with cell aspect ratio. Empirically, we have found a modified timestep number of

$$\delta t = \left(\frac{\min(\lambda_M)}{\max(u_{rms})} \right) \left(\frac{\min(\lambda_M)}{\max(\lambda_M)} \right)^{1/2} \quad (13)$$

is sufficient to prevent this energy pileup. Apparently, standard CFL considerations lead to temporal filtering of fine scales of motion that are necessary to dissipation energy at the cutoff which are not reflected in the maximum u_{rms} .

References

- [1] M. Germano, U. Piomelli, P. Moin, and W. H. Cabot, “A dynamic subgrid-scale eddy viscosity model,” *Physics of Fluids A: Fluid Dynamics*, vol. 3, p. 1760, 1991.
- [2] U. Piomelli and E. Balaras, “Wall-layer models for large-eddy simulations,” *Annual Review of Fluid Mechanics*, vol. 34, pp. 349–374, 2002.
- [3] A. Scotti, C. Meneveau, and D. K. Lilly, “Generalized Smagorinsky model for anisotropic grids,” *Physics of Fluids A*, vol. 5, p. 2306, 1993.
- [4] A. Vreman, “An eddy-viscosity subgrid-scale model for turbulent shear flow,” *Physics of Fluids*, vol. 16, no. 10, pp. 3670–3681, 2004.
- [5] W. Rozema, H. J. Bae, P. Moin, and R. Verstappen, “Minimum-dissipation models for large-eddy simulation,” *Physics of Fluids*, vol. 27, 2015.
- [6] A. Misra and D. Pullin, “A vortex-based subgrid stress model for large-eddy simulation,” *Physics of Fluids*, vol. 9, pp. 2443–2454, 1997.
- [7] J. Jiménez and R. D. Moser, “Large-eddy simulations: Where are we and what can we expect?,” *AIAA Journal*, vol. 28, no. 4, pp. 605–612, 2000.
- [8] J. Smagorinsky, “General circulation experiments with the primitive equations. i. the basic experiment,” *Mon. Weather Rev.*, vol. 91, pp. 99–164, 1963.
- [9] M. Lee and R. D. Moser, “Direct numerical simulation of turbulent channel flow up to $Re=5200$,” *Journal of Fluid Mechanics*, vol. 774, pp. 395–415, 7 2015.
- [10] J. L. Synge and A. Schild, *Tensor Calculus*. Dover, 1949.
- [11] V. Eswaran and S. B. Pope, “An examination of forcing in direct numerical simulations of turbulence,” *Computers and Fluids*, vol. 16, no. 3, pp. 257–278, 1988.